A quantitative analysis of grid-related systematic errors in oxidising capacity and ozone production rates in chemistry transport models

J. G. Esler, G. J. Roelofs, M. O. Köhler, F. M. O'Connor

Atmos. Chem. Phys. Discuss., 4, 2533–2568, 2004
www.atmos-chem-phys.org/acpd/4/2533/
SRef-ID: 1680-7375/acpd/2004-4-2533

Atmospheric Chemistry and Physics Discussions

A quantitative analysis of grid-related systematic errors in oxidising capacity and ozone production rates in chemistry transport models

J. G. Esler[1], G. J. Roelofs[2], M. O. Köhler[3], and F. M. O'Connor[3]

[1]Department of Mathematics, University College London, UK
[2]Institute for Marine and Atmospheric research, Utrecht – IMAU, The Netherlands
[3]Centre for Atmospheric Science, University of Cambridge, Cambridge, UK

Received: 8 February 2004 – Accepted: 14 April 2004 – Published: 12 May 2004

Correspondence to: J. G. Esler (gavin@math.ucl.ac.uk)

Abstract

Limited resolution in chemistry transport models (CTMs) is necessarily associated with systematic errors in the calculated chemistry, due to the artificial mixing of species on the scale of the model grid (grid-averaging). Here, the errors in calculated hydroxyl radical (OH) concentrations and ozone production rates $P(O_3)$ are investigated quantitatively using both direct observations and model results. Photochemical steady-state models of radical chemistry are exploited in each case to examine the effect on both OH and $P(O_3)$ of averaging relatively long-lived precursor species, such as O_3, NO_x, CO, H_2O, etc., over different spatial scales. Changes in modelled $P(O_3)$ are estimated, independently of other model errors, by calculating the systematic effect of spatial averaging on the ozone production efficiency ϵ_N, defined as the ratio of ozone molecules produced per NO_x molecule destroyed. Firstly, an investigation of in-flight measurements suggests that, at least in the northern midlatitude upper-troposphere / lower stratosphere, averaging precursor species on the scale of a T42 grid ($2.75^\circ \times 2.75^\circ$) leads to a 15–20% increase in OH concentrations and a 5–10% increase in ϵ_N. Secondly, results from CTM model experiments are compared at different horizontal resolutions. Low resolution experiments are found to have significantly higher [OH] and $P(O_3)$ compared with high resolution experiments. The degree to which these differences may be explained by the systematic error associated with the model grid size is investigated by degrading the high resolution data onto a low resolution grid and then recalculating ϵ_N and [OH]. The change in calculated ϵ_N is found to be significant and can account for much of the difference in $P(O_3)$ between the high and low resolution experiments. The calculated change in [OH] is less than the difference in [OH] found between the experiments, although the shortfall is likely to be due to the indirect effect of the change in modelled NO_x, which is not accounted for in the calculation. It is argued that systematic errors caused by limited resolution need to be considered when evaluating the relative impacts of different pollutant sources on tropospheric ozone.

ACPD

4, 2533–2568, 2004

1. Introduction

The nonlinearity inherent in the atmospheric photochemical system ensures that it is sensitive to mixing effects. For example, the ozone production efficiency ϵ_N, defined as the ratio of ozone molecules produced per nitrogen oxide (NO_x=NO+NO_2) molecule destroyed (Lui et al., 1987; Lin et al., 1988) is known to increase with the rate that NO_x emissions are mixed into the environment (Chatfield and Delaney, 1990; Jacob et al., 1993; Poppe et al., 1998). Esler et al. (2001) have demonstrated that, in particular, hydroxyl radical (OH) levels are sensitive to mixing between tropospheric and stratospheric air. Radical species such as OH cannot be considered conserved under mixing processes, at least on timescales greater than their chemical lifetime (typically a few seconds in the case of OH), as they adjust to a local photochemical equilibrium that depends nonlinearly on the concentrations of their longer-lived precursor species (e.g. O_3, CO, NO_x, and H_2O).

Sensitivity to mixing has well-known implications for chemistry transport models (CTMs), as mixing ratios are generally assumed constant in model grid-boxes. This raises the possibility that, because variations on the sub-grid scale are not represented, systematic errors may result in CTM chemical budgets (Pyle and Zavody, 1990). This paper addresses this issue, by concentrating on quantifying model error in calculated ozone production rates $P(O_3)$, and in OH concentrations, caused by the finite resolution of the model grid. Understanding and evaluating these systematic errors will be of lasting interest to the modelling community as recent increases in computational power have coincided with increased interest in longer time-scale "chemistry-climate" experiments, suggesting that a large range of model resolutions will be utilised in future studies.

The total ozone production in a given region can be estimated from the total NO_x source using the (appropriately averaged) ozone production efficiency ϵ_N in that region

ACPD
4, 2533–2568, 2004

(Lui et al., 1987). The ozone production efficiency is calculated using

$$\epsilon_N \equiv \frac{P(O_3)}{L(NO_x)}, \quad (1)$$

where $L(NO_x)$ is the rate of loss of NO_x. The extent to which ϵ_N is sensitive to the effects of spatial averaging on model chemical fields can therefore be used to estimate the sensitivity of total ozone production to a change in the model resolution, under conditions where the model transport and chemical sources (particularly of NO_x) remain invariant under the resolution change. By recalculating ϵ_N for otherwise identical chemical fields, when they are interpolated onto different model grids, the systematic error due to the effect of spatial averaging on the model chemistry can be isolated and compared in magnitude to other potential sources of model error.

As will be described in Sect. 2, photochemical steady state models are used to estimate the net change in ϵ_N and [OH] when observed or modelled precursor fields are averaged on scales corresponding to CTM model grid-boxes at different horizontal resolutions (referred to as grid-averaging hereafter). It is to be emphasised that the objective of the study is to estimate the direct effect of a resolution change on CTM chemical budgets in an idealised situation where no changes in model transport, chemical sources or parameterisations accompany the resolution change. Two separate studies are made, the first an analysis of in-flight observations, and the second a detailed investigation into the differences between CTM experiments at different horizontal resolutions.

In Sect. 3 we analyse in-flight measurements from the upper troposphere-lower stratosphere (UTLS) region made during the SONEX aircraft campaign (13 October to 12 November 1997; J. Geophys. Res., 105, issue D3, 2000). Data from 14 flights from Shannon, Ireland (52° N, 10° W) and Bangor, Maine (45° N, 68° W) have been used. This data is not quite a statistically representative sample of late autumn/early winter UTLS conditions throughout the northern midlatitudes, as it is biased towards the North Atlantic flight corridor where polluted airmasses will be encountered more frequently. However, because of the layered nature of the airmasses in the extratropics

(Thouret et al., 2000), a large number of distinct airmasses have been sampled on these flights, and the data contains a great deal of representative information about
(i) The spatial scales of variation of each precursor species.
(ii) The correlations between different precursor species.
The sensitivity of the mean value of ϵ_N and total [OH] to the spatial resolution of the data depend crucially on the measured statistics of (i) and (ii).

Section 4 contains a comparative study of one month (January and July) datasets from model experiments made at different horizontal resolutions. Two different models from the Cambridge (TOMCAT) and Hamburg-Utrecht (ECHAM4) groups have been used. TOMCAT is an offline chemistry transport model driven directly by meteorological analyses, whereas ECHAM4 is primarily a general circulation model. In the experiments we will consider, however, ECHAM4 is forced by a relaxation to meteorological analysis, and hence in this mode operates essentially as a chemistry transport model that may be compared directly with TOMCAT. More details on the models will be given in Sect. 2. The differences between modelled $P(O_3)$ and OH between low and high resolution runs are described and analysed. One central question to be addressed is the extent to which the differences in $P(O_3)$ and OH are directly due to "grid-averaging" of the precursor fields, compared to how much is due to other differences in the model set-up caused by the change in resolution. To answer this question, the methodology to be adopted is designed to estimate the magnitude of the grid-related error in the absence of other possible changes that may be caused by a change in model horizontal resolution. Examples of the possible changes that may take place are differences in model transport, especially stratosphere-troposphere exchange (STE hereafter) (Kentarchos et al., 2000) changes in the parameterisations of convective transport and turbulent mixing (Tiedtke, 1989), changes to the parameterised source of NO_x from lightning, and alterations to emissions inventories to fit the new model grid. Errors due to incorrect STE, convection, lightning etc. may be of indeterminant sign, may be sensitive to technical issues (e.g. model upper boundary conditions), and increases in model resolution may not necessarily act to reduce their magnitude. By contrast, as will be

shown, the grid-averaging error in the model chemistry will be systematically reduced as resolution is increased. However, some grid-averaging error is likely to persist for the foreseeable future, so we therefore aim to evaluate the magnitude of the errors in $P(O_3)$ and OH associated with grid-averaging, independently of the other model errors which have unknown resolution dependence.

In the conclusions in Sect. 5 we discuss the implications of the results.

2. Methodology

2.1. Photochemical steady state approximations

Both the analysis of in-flight observations in Sect. 3 and CTM experiments in Sect. 4 depend on the use of photochemical steady state (PCSS) approximations, in order to model total changes to OH and ozone production efficiency ϵ_N caused by grid-averaging of the precursor species on different spatial scales. The PCSS schemes are useful as they allow equilibrium concentrations of radical species to be calculated both before and after mixing or averaging processes are applied to the precursor fields. The change in the calculated equilibrium PCSS radical concentrations corresponds to the change in radical concentrations that would occur once the radical species have "adjusted" to their new local precursor concentrations (this adjustment would, in reality, take place on the timescale of the chemical lifetime of the radical species). Use of PCSS schemes therefore allows systematic changes in radical concentrations, $P(O_3)$, $L(NO_x)$ and hence ϵ_N, caused by grid-averaging to be quantified.

Two different PCSS schemes are used, referred to as the "UTLS scheme", and the "full scheme", and both are described in more detail in the appendix. The UTLS scheme is designed to model the essential components of the radical chemistry taking place in the midlatitude UTLS where the SONEX flights took place. The UTLS scheme steady-state expressions allow [OH] and $P(O_3)$ to be straightforwardly calculated given the concentrations of the precursors NO, O_3, CO and H_2O from the SONEX in-flight

measurements.

As an example of the utility of the UTLS scheme, Fig. 1a and b show the extent of agreement with SONEX measurements of [OH] and [HO_2] during flight 13 (10 November 1997) of the campaign. By contrast, the full scheme is designed to give good correlations with the full TOMCAT radical chemistry throughout the troposphere. It considers more reactions and species than the UTLS scheme whilst still representing a significant reduction in complexity compared to the full TOMCAT chemistry. In Fig. 1c–e comparisons between the UTLS scheme, the full scheme, and actual TOMCAT [OH] and [HO_2] are shown. In panels (c)–(d), a comparison between TOMCAT global mean [OH] and [HO_2] and the reduced steady-state schemes are shown as a function of height. Global mean [HO_2] is modelled well by both schemes, but the full scheme overestimates [OH]/[HO_2], whilst the UTLS scheme underestimates it. Correlations between TOMCAT [OH] and [HO_2] and calculated values of [OH] and [HO_2] are shown in panel (e). The full scheme gives correlations above 0.995 in the mid and upper troposphere, but the correlations decrease near the surface where reactions involving neglected species become more important. The UTLS scheme also does better in the UTLS compared with the lower troposphere, as intended, because for this scheme the neglected reactions become increasingly important in the lower troposphere. Overall, the very high correlations give confidence that changes in calculated PCSS [OH] and [HO_2] under grid-averaging will be comparable to changes in [OH] and [HO_2] in the actual CTM.

Figure 2 illustrates the dependence of ϵ_N, $P(O_3)$, [HO_2] and [OH] on NO_x concentrations in the UTLS scheme described above, and is plotted to illustrate schematically how grid-averaging can lead to systematic changes in mean radical concentrations. Note that the quantities plotted also depend nonlinearly on the concentrations of other species, which may modify the simple picture described below, but the primary nonlinearity in each case is with respect to NO_x. Consider two air parcels "A" and "B", that are identical except for different NO_x concentrations of 20 pptv and 500 pptv respectively, and which are resolved separately at a given model resolution. The mean [OH], [HO_2]

or $P(O_3)$ between the two parcels will lie somewhere on the dashed lines in Fig. 2 (depending on the relative sizes of the parcels). Supposing then that a lower resolution simulation cannot then resolve both "A" and "B" separately and effectively mixes them together in a single grid-box. The net changes in [OH], [HO_2] and $P(O_3)$ that ensue are illustrated by the black arrows on Fig. 2. The systematic effect is clearly to increase [OH] and $P(O_3)$ and decrease [HO_2]. Although radical concentrations depend to an extent on other precursor species, it is the averaging of the NO_x field that causes the largest systematic error. This has been tested by repeating some of the calculations in Sects. 3 and 4 below but with grid-averaging applied to the NO_x field only, with largely similar results.

Evaluation of the change in ϵ_N under mixing between the two parcels needs further consideration. In this case the relevant quantity is not the mean value of ϵ_N between the two parcels, but a weighted mean, taking account of the fact that more NO_x molecules may be lost in one parcel than the other. Using an overbar to denote a typical averaging operation, such as the mean between "A" and "B", a time-mean, or a zonal mean, the appropriate weighted mean for ϵ_N can then be written

$$< \epsilon_N >= \frac{\overline{\epsilon_N \quad L(NO_x)}}{\overline{L(NO_x)}} = \frac{\overline{P(O_3)}}{\overline{L(NO_x)}} \tag{2}$$

The weighted mean $<\epsilon_N>$, is then a true measure of the mean number of ozone molecules produced per NO_x molecule destroyed in the two parcels, or in the wider domain. In Sects. 3 and 4, where mean values of ϵ_N are quoted, it is the weighted mean $<\epsilon_N>$ that is implied.

2.2. Methodology as applied to SONEX observations

In order to investigate the effect of spatial averaging on radical concentrations we have applied the following methodology to the SONEX data described in Sect. 1. Crowther et al. (2002) have recently used a similar technique to consider the effect of mixing on

hydroxyl radical production $P(OH)$. It is important to emphasise at this stage that the methodology described below has a different objective compared with direct model-observation comparison studies, e.g. Brunner et al. (2003). Model-observation comparisons aim to quantify the total CTM error, whereas the grid-averaging technique described below aims to isolate and quantify the CTM error due to grid-averaging of the radical precursor fields.

In practice, the measured fields of O_3, CO, H_2O and NO_x are averaged as follows. Using an estimate of aircraft speed (200 ms^{-1}), CTM grid-box sizes of 5.5°, 2.75°, 1.375°, 0.688°, and 0.344° (corresponding to spectral resolutions T21, T42, T85, T170 and T341) are converted to time intervals. The data is then averaged over these time intervals. Numerical diffusion in any CTM advection scheme invariably acts to diffuse strong gradients between adjacent grid-boxes, and to simulate this effect we apply a further smoothing operation, replacing the concentration χ_N in the Nth interval of each species according to

$$\chi_N \rightarrow 0.25\chi_{N-1} + 0.5\chi_N + 0.25\chi_{N+1}. \quad (3)$$

Figure 3a shows measured $[O_3]$ from flight 13 along with examples of the resulting averaged O_3 fields at T170 and T42 scales. Note that, unlike the radical concentrations, the total amount of each precursor species (integrated along each flight track) is conserved by the averaging process. The mean [OH], $[HO_2]$ and $P(O_3)$ for all of the flights are then calculated using the UTLS scheme for each averaging scale in turn. Fixed reaction rates calculated at typical UTLS conditions (240 K and 300 hPa) (DeMore et al., 1997) and fixed photolysis rates are used in these calculations. To confirm that the results are insensitive to reaction rates the tests were repeated with rates calculated at (220 K, 200 hPa) and (260 K, 600 hPa) in turn, with similar results found.

2.3. Methodology as applied to CTM results

In Sect. 4 below we analyse low and high resolution CTM experiments for January and July 1996, using sets of experiments that differ in horizontal resolution. Grid-averaging

due to changes in vertical resolution might be expected to have a similar effect to the changes in horizontal resolution described below, but are not considered here. Testing hypothesis related to vertical resolution may prove more difficult, as changes usually coincide with separate changes to model physics.

As discussed above, the two models used are the Cambridge off-line chemistry transport model (TOMCAT), (Stockwell and Chipperfield, 1999) and the European Centre Hamburg Model version 4 (ECHAM4), (Roeckner et al., 1996; Roelofs and Lelieveld, 2000). The TOMCAT experiments were executed at T42 L31 (approximately 2.75°×2.75°) and T21 L31 (5.5°×5.5°) resolution respectively. Of the 31 model levels, 26 are located between the surface and 100 hPa. In contrast ECHAM4 is run at higher horizontal resolution, T63 (1.875°×1.875°) and T30 (3.75°×3.75°), but lower vertical resolution L19, with 15 levels between the surface and 100 hPa. The TOMCAT simulations are forced by ECMWF operational analyses. ECHAM4 differs from TOMCAT in that it is primarily designed to operate as a general circulation model (GCM), although in this configuration it uses a Newtonian relaxation to nudge vorticity, divergence, temperature and surface pressure towards the ECMWF analyses (Kentarchos et al., 2000).

The primary purpose of the analysis is to determine the extent to which differences between OH and $P(O_3)$ at low and high resolution can be accounted for as being purely due to the effects of grid-averaging on long-lived precursor species. To separate out the direct effect on OH and $P(O_3)$ of grid-averaging we proceed as follows. Taking high resolution data, such as T42 ozone in TOMCAT (O_3:T42), a "degraded" field (O_3:T42D) is created by interpolating the T42 field onto a lower resolution grid, in this case T21. The interpolation routine is designed to act conservatively, so that for example the total ozone on any model level is unchanged when the data is degraded onto a coarser grid. Figure 3b and c show O_3:T42 and O_3:T42D from TOMCAT data on 29 July 1996 (the model level is around 700 hPa). The full PCSS scheme described above can be used to calculate monthly mean[1] [OH] and ϵ_N both from the T42 fields and the

[1]Because of the large amounts of data involved monthly means are generally calculated

degraded T42D fields. The differences between the respective calculations represent a systematic change in the model chemistry caused by grid-averaging alone. The calculated change in [OH] and $P(O_3)$ under grid-averaging may then be compared to the actual differences in [OH] and $P(O_3)$ between low and high resolution experiments, to determine the extent to which grid-averaging accounts for the differences between the model runs. As with the SONEX data, there is the question of both the direct effect of grid-averaging on [OH] and $P(O_3)$ and the indirect effect due to the change in NO_x concentrations induced by grid-averaging. To account for the indirect effect, we also calculate changes in the ozone production efficiency ϵ_N under grid-averaging, taking the weighted average as described above.

Finally, we exploit a similar methodology to examine how changes in the transport of stratospheric ozone contribute to differences in $P(O_3)$ and [OH]. In TOMCAT we exploit the artificial stratospheric ozone tracer (O_3s hereafter), which is designed to behave like ozone except that sources associated with production in the troposphere are omitted (Plantevin, 1999). O_3s can be used to quantify differences in tropospheric ozone due to changes in transport from the stratosphere (Roelofs and Lelieveld, 1997). A new ozone field can be created by subtracting O_3s from O_3 in the T42 data and adding O_3s from the corresponding T21 experiment. The change in calculated [OH] and $P(O_3)$ when this new ozone field is used in place of the original T42 field can be interpreted as the change in [OH] and $P(O_3)$ that can be explained by the difference in stratospheric ozone transport between the two model runs.

from 4 days of data output on the 1st, 11th, 21st and 31st of the month in question, using fields from 00:00 UT, 06:00 UT, 12:00 UT and 18:00 UT. However the monthly means calculated in this fashion were robust in the sense that near identical results were obtained when either more days or fewer days of data were used.

3. Results: Analysis of SONEX Observations

Figure 4 shows how the calculated $P(OH)$, [OH], [HO_2], ϵ_N, $P(O_3)$ and $L(O_3)$ vary as the spatial averaging distance (grid-box size) is varied. The UTLS scheme is used to derive the calculated values in each case, with constant reaction and photolysis rates typical of SONEX conditions used (see caption). Results are expressed as a percentage change, relative to the calculated values for the fully resolved data, and these calculated values are printed on each panel. The results are robust in the sense that spatial averaging has a systematic effect that increases with the averaging scale, and this systematic effect can be seen separately in the data from each individual flight. The three curves on each plot correspond to results from all flights (diamonds), those flights encountering mainly marine conditions (triangles, flights with mean [NO_x]<150 pptv) and those flights encountering continental influence (stars, mean [NO_x]≥150 pptv). The distinction between marine and continental flights is made in order to demonstrate that results are not heavily dependent on those SONEX flights that intercept heavily polluted airmasses around North America and the North Atlantic flight corridor. Arguably, the "marine" flights (triangles) are more representative of the midlatitude UTLS as a whole, and when comparing results with the CTM results of Sect. 4 below we have considered the difference between the T21 and T42 "triangle" points on each plot.

The results in Fig. 4 can be summarised as follows:

- Hydroxyl radical production $P(OH)$ increases due to grid-averaging by up to 10% (for T21), as has been discussed in detail by Crowther et al. (2002). Using an analysis based on MOZAIC aircraft measurements, they note that the increase in $P(OH)$ is maximum near the tropopause, where large variances in [O_3] and [H_2O] are encountered. [O_3] and [H_2O] are anticorrelated in the UTLS and the effect of grid-averaging is to decrease this anticorrelation, increasing $P(OH)$.

- Hydroxyl radical concentrations [OH] are increased by 20–25% (for T21). Increased $P(OH)$ accounts for only 7–8% of the 20–25% increase, since [OH]=R_H

ACPD
4, 2533–2568, 2004

$[HO_2]$ is not a linear function of $P(OH)$ in PCSS expressions given in the appendix. The remaining increase in [OH] is in fact due to the mixing of NO_x by the grid-averaging process. From Fig. 2, mixing between two otherwise similar air parcels with different NO_x concentrations will lead to increased total OH as the [OH]-[NO_x] curve is convex, i.e. $\partial^2[OH]/\partial[NO_x]^2<0$. If grid-averaging is applied only to the NO_x field, and not to other species, comparable increases in [OH] are still observed. In polluted conditions hydro-peroxy radical concentrations $[HO_2]$ are reduced by grid-averaging, and following similar arguments it may be deduced from Fig. 2 that this reduction may also be caused by the mixing of NO_x.

– Grid-averaging leads to a systematic increase of ozone production efficiency ϵ_N. One direct effect of grid-averaging is to reduce the negative correlation between [NO] and $[HO_2]$, increasing $P(O_3)$ directly. Grid-averaging acts to increase $L(NO_x)$ (not shown) for SONEX data, hence the increase in ϵ_N of 5–15% (at T21) is less than the direct 15–25% increase in $P(O_3)$. Loss rates of ozone $L(O_3)$ are slightly increased by grid-averaging, but the change is relatively small compared with the change in $P(O_3)$.

These statistics are of course valid only for the northern midlatitude UTLS for the season of the SONEX flights (October-November). To estimate the extent to which the above results may be extrapolated to the rest of the troposphere, in Sect. 4 below we have applied a similar grid-averaging technique to data from CTMs.

4. Results: analysis of CTM Experiments

4.1. TOMCAT Experiments

In this section we compare results from the high (T42) and low (T21) TOMCAT experiments for January and July 1996 described in Sect. 2 above. Apart from the resolution

of the grid, the experiments have an identical period of integration and near identical surface and aircraft emissions, which differ only in respect of details relating to the model grid. The experiments are therefore suitable for a detailed investigation using the methodology described in Sect. 2. The aim is to determine as far as possible the extent to which differences in the modelled [OH] and $P(O_3)$ between the two simulations can be systematically explained by:

1. Grid-averaging effects caused by the chemistry calculations taking place on the different horizontal scales of the model grid in each experiment;

2. Differences in the transport of ozone from stratosphere to troposphere between the two experiments (e.g. Kentarchos et al., 2000)

or whether the differences must be due to other changes, such as systematic changes in the parameterisations of convection, turbulent mixing or the source of NO_x due to lightning.

Figure 5a shows the difference in $P(O_3)$ between the July 1996 monthly mean T21 and T42 TOMCAT simulations. The T21 experiment is characterised by regions of significantly increased production, notably in the tropics to the north of the equator, in the extratropical lower troposphere in both hemispheres, and at high latitudes in the summer hemisphere upper troposphere. There are also regions of reduced production in the mid and upper troposphere in both hemispheres. To determine the degree to which these differences in $P(O_3)$ between the two experiments can be explained purely in terms of the effect of grid-averaging on the chemistry, calculated ozone production efficiency ϵ_N can be compared between the T42 fields and the degraded "T42D" fields. The percentage change in calculated ϵ_N when the degraded T42D fields were used is shown in Fig. 5b (note the same contour interval as before). The weighted mean value of ϵ_N is clearly increased by grid-averaging, particularly throughout the tropics and in the southern hemisphere lower troposphere. Comparing the spatial patterns of the change in ϵ_N shown in Fig. 5b with the change in $P(O_3)$ shown in Fig. 5a, it is clear that much of the increased $P(O_3)$ in the T21 experiment compared with the T42 experiment

ACPD
4, 2533–2568, 2004

may be explained by increased ozone production efficiency due to grid-averaging. Note that the spatial patterns should not be expected to correspond exactly as transport, as well as the model treatment of NO_x buffer species such as PAN and HNO_3, must play a role in modifying the pattern of $P(O_3)$ in Fig. 5a in response to the changes in ozone production efficiency shown in Fig. 5b. Figure 5c shows the calculated July mean values of ϵ_N for the T42 experiment. As expected from Fig. 2a, ϵ_N is smallest where NO_x concentrations are highest (in the northern midlatitude boundary layer) and largest in the southern hemisphere in the midlatitude upper troposphere.

A similar analysis has been used to investigate changes in OH, with the results shown in Fig. 6. Panel (a) shows the zonal mean OH concentration in pptv in the T42 July monthly mean, with the percentage change between T21 and T42 shown in Fig. 6b. [OH] is higher in the T21 simulation almost everywhere, particularly throughout the middle and upper troposphere. Figure 6c shows the change in calculated [OH] due to grid-averaging (more contours have been added, although the colour scheme is as in panel b). The direct effect of grid-averaging on [OH] does not account for more than around 20–25% of the difference between the T21 and T42 experiments. However, as will be argued below, much of the remaining difference may be accounted for by the indirect effect of grid-averaging on NO_x concentrations. Note that direct increases in [OH] in the northern UTLS of 3–5% for the degraded T42D fields are again broadly consistent with the results of the observational study shown in Fig. 4.

Crowther et al. (2002) have suggested that model grid-averaging causes systematic errors in CTM chemistry by effectively mixing dry, O_3-rich air and moist O_3-poor air, thereby reducing the anti-correlation between O_3 and H_2O in the tropopause region, and generating increased hydroxyl radical production P(OH). In order to isolate and quantify the effect of grid-averaging on P(OH), we have calculated P(OH) using the degraded T42D fields. Compared with P(OH) calculated from the standard T42 fields, P(OH) is indeed increased by grid-averaging in the tropopause region by a few per-cent (not shown). To evaluate the direct effect of the increase in P(OH) on oxidising capacity, PCSS scheme was used to calculate [OH] with P(OH) calculated from the the

T42D (grid-averaged) data, and the remaining precursor concentrations taken from the standard T42 fields. The results can then compared with the [OH] calculated from the standard T42 fields with standard T42 P(OH). This comparison is shown in Fig. 6d. As with the SONEX data, only around one-third of the total increase in [OH] due to grid-averaging (shown in Fig. 6c) can be accounted for by increased P(OH). Grid-averaging leads to systematic errors in [OH] concentration even when P(OH) is held constant, due to changes in R_H=[OH]/[HO_2], for example, which is strongly determined by [NO_x]. Our results therefore suggest that [OH] is more sensitive to errors in calculated R_H compared to calculated P(OH).

Clearly, any change in global NO_x concentrations is of central importance for global [OH] and $P(O_3)$, and the difference in NO_x distributions between the model experiments merits further investigation. If sources are held constant, global NO_x distributions are largely determined by the loss reaction in $L(NO_x)$, (see appendix for definition). From Eq. (1) it is clear that changes in $L(NO_x)$ will be closely related to changes in ϵ_N described above. How $L(NO_x)$ varies under grid-averaging is therefore of central importance to how CTM chemistry will be affected by a change in resolution.

Figure 7a shows how July mean NO_x changes between the T21 and T42 simulations. The pattern of increase in NO_x corresponds closely to the increase in $P(O_3)$ described in connection with Fig. 5. In Fig. 7b, the change in $L(NO_x)$ due to grid-averaging is shown. $L(NO_x)$ is decreased in most regions with a spatial pattern that anticorrelates closely with the increase in ϵ_N shown in Fig. 5b. Grid-averaging therefore has a substantial impact on NO_x destruction, with typical NO_x lifetimes being longer at lower resolution. Increased NO_x at low resolution is then primarily responsible for increased $P(O_3)$, and must also contribute significantly to increased [OH] as shown in Fig. 6b.

As stated above, an alternative hypothesis for the changes in oxidising capacity and $P(O_3)$ between model runs is that they are directly related to a change in the magnitude of STE. An increase in STE is of course associated with an increase in stratospheric ozone transported into the troposphere, and the artificial "stratospheric ozone tracer" O_3s in TOMCAT (Plantevin, 1999) can be exploited in order to evaluate the magnitude

of this change.

Figure 8a shows the difference in O_3s between T21 and T42 simulations. STE in the T21 experiment is significantly weaker, the cross-tropopause flux of ozone is 815 Tg yr^{-1} in the T42 simulation (O'Connor et al., 2004), and only 465 Tg yr^{-1} in the T21 simulation (Cobb, 2002). Hence in the T21 simulation, in the extratropical lower troposphere O_3s is lower in the July mean, and there is significantly higher O_3s in the UTLS region. In order to isolate and quantify the implications of the change in O_3s for modelled [OH] and $P(O_3)$, we calculated [OH] and $P(O_3)$ for the T42 fields with a modified ozone field. The modified ozone field is created by subtracting out T42 O_3s and replacing it with T21 O_3s. The changes in calculated [OH] and $P(O_3)$ when the modified ozone field is used are shown in Figs. 8b and c, and are seen to be small at low latitudes. At high latitudes decreased STE leads to lower tropospheric OH and $P(O_3)$ in the lower troposphere with the opposite signal in the UTLS. Overall, comparing Figs. 8b and c with 6b and 5a, the change in O_3s due to decreased STE does not contribute significantly to the difference between [OH] and $P(O_3)$ in the T21 and T42 experiments.

All of the calculations described in this section were repeated for January, with largely similar results. By way of example, Fig. 9 presents the same analysis for the January mean OH that was shown in Fig. 6 for the July case. Figure 9a shows the T42 January mean, with the systematic difference between the T21 and T42 experiments shown in Fig. 9b. Figure 9c shows the proportion of the change in OH that can be explained by the direct effect of grid-averaging (as in the July case, it is around one third of the total change). Figure 9d shows the net effect of grid-averaging applied to P(OH) alone, as in Fig. 6. When the grid-averaging technique is applied to January data (not shown), a similar picture of increased [OH], $P(O_3)$ and ϵ_N, consistent with decreased $L(NO_x)$, is found as with the July case.

4.2. ECHAM4 experiments

To investigate the degree to which the above results were model dependent, the analysis was repeated for the chemistry-GCM ECHAM4. High (T63) and low (T30) resolution

model experiments were analysed (Kentarchos et al., 2000).

Figure 10 shows the results for $P(O_3)$ in ECHAM4, and can be compared directly with Fig. 5 for TOMCAT. In Fig. 10a it is clear that there is a very large change in $P(O_3)$ between the ECHAM4 simulations. This change occurs because the total sources of NO_x, particularly from lightning, in ECHAM4 are not constrained to remain invariant under the change in resolution to the extent they are in TOMCAT. NO_x concentrations (not shown) are much higher in the low resolution (T30) experiment, particularly away from regions of tropical convection. Figure 10b shows the change in ϵ_N when degraded data (T63D) is used in place of the full T63 fields, and confirms that grid-averaging cannot explain the differences in $P(O_3)$ between the simulations. Comparing Fig. 10b with Fig. 5b, there is a similar increase in ϵ_N in the tropics associated with the grid-averaging but, unlike in TOMCAT, grid-averaging in ECHAM4 has little effect in the extratropics. One possible reason for the small grid-averaging effect in the extratropics in ECHAM4 is that vertical transport is more diffusive compared with TOMCAT due to the lower vertical resolution. ECHAM4 appears to be less successful than TOMCAT in modelling transport of pollutants out of the extratropical boundary layer in large-scale plumes (Brunner et al., 1998), and hence has lower variances in NO_x concentrations in the extratropical mid and upper troposphere. In the tropics, by contrast, much of the vertical transport of NO_x takes place in vertical columns through the convective parameterisation.

Comparing Fig. 10c and Fig. 5c, it is interesting to note the significantly higher mean values of ϵ_N everywhere in the troposphere in ECHAM4 compared with TOMCAT. This is due in part to lower mean NO_x concentrations in ECHAM4, with lower variances in NO_x distributions outside the boundary layer also being important.

5. Conclusions

In this paper both observational data and model simulations have been used to quantify systematic errors in CTM chemistry associated with the averaging of chemical fields

on the scale of the model grid. The magnitude of the predicted trends depend on the variance of precursor species concentrations, particularly of NO_x, and the correlations between precursors as well as local reaction and photolysis rates. Hence the predicted trends vary with latitude and height, but in most locations are large enough to make a significant contribution to the actual differences between CTM model experiments executed at different resolutions. In TOMCAT in particular, the predicted change in ϵ_N obtained by degrading T42 data (up to 15% in the tropical upper troposphere, 20–30% in the winter extratropical lower troposphere) was found to be comparable in magnitude to the actual difference in $P(O_3)$ between the T42 and T21 simulations.

There are several implications for modellers. Firstly, based on the analysis of SONEX observations described in Sect. 3 (see Fig. 4), the systematic difference between [OH] and $P(O_3)$ calculated at T42 and T21, represents only around a third to a half of the difference between T42 and the fully resolved data. It therefore seems reasonable to conclude that the differences between the T21 and T42 simulations reported in Sect. 4 are considerably smaller than the differences between the T42 simulation and "reality". This point must be emphasised as we have not even considered the related issue of changing the vertical resolution between model experiments, which will further increase the effect of "grid-averaging". Secondly, from Fig. 8 and the surrounding discussion, we have shown that the effect of increased tropospheric ozone in the T42 experiment due to enhanced stratosphere-troposphere exchange (STE) has a minimal impact on the radical chemistry and $P(O_3)$ compared with the effect of grid-averaging the T42 fields. It is therefore the case that even a relatively large change in modelled STE, as occurred between the TOMCAT T42 and T21 simulations, cannot be considered to have a large knock-on effect on model chemistry, at least when compared with the known grid-based model errors. Finally, it is worth noting that the significant grid-related trend towards lower NO_x, as resolution increases, that is suggested by Fig. 7, may be a factor in the comparatively poor performance of most CTMs in quantitatively modelling this species throughout the troposphere (Brunner et al., 2003).

Trends towards higher concentrations of hydrocarbons and CO will also accompany

the trend towards lower OH. Models will only strictly approach the appropriate chemical equilibrium in response to a change in resolution on the time-scale of the chemical eigenstate associated with methane (~14 years) (Prather, 1994), and significant adjustments to species other than methane (such as CO and O_3) may also occur on this timescale (Wild and Prather, 2000). Recent parallelisation means that TOMCAT integrations at resolutions of T106 L50 and higher are now possible, and this study makes it possible to anticipate some of the changes associated with the large improvement in resolution.

It is important to emphasise that ozone in the troposphere is significantly buffered, so that, for example, a sustained 10% increase in $P(O_3)$ everywhere will generate a significantly smaller percentage increase in the burden of tropospheric ozone. This is easily explained as additional ozone contributes to the HO_x budget and hence its own destruction. Therefore, substantial errors in modelled values of ϵ_N for some NO_x sources in a CTM are not necessarily associated with large errors in the modelled ozone fields themselves. While the overall accuracy of modelled ozone fields (Law et al., 2000) is superficially reassuring, important questions remain about the relative importance of different NO_x sources for the overall ozone budget. While a CTM experiment will model ϵ_N accurately for a widely dispersed source, it will not do so for a local, concentrated source such as an aircraft or ship plume. The systematic errors we have described may therefore be most relevant, for example, in the case of CTM experiments designed to evaluate the relative contributions of different NO_x sources to the tropospheric ozone budget (Lelieveld and Dentener, 2000; Wild et al., 2001). This problem has been recognised, and solutions such as nested-grids near sources (Sillman et al., 1990; Jacob et al., 1993) and aircraft plume parameterisations (Kraabøl et al., 2000) have been proposed, but a detailed understanding of the importance and magnitude of such systematic errors, as well as the extent to which the above solutions are effective, has yet to be established.

ACPD
4, 2533–2568, 2004

Appendix: Photochemical Steady-State Models

In this appendix we state the PCSS expressions used to calculate radical concentrations from the concentrations of precursor species as detailed below. The expressions are derived following the standard approach (Poppe et al., 1995).

5.1. UTLS scheme

The UTLS scheme is used to derive [OH], [HO_2], $P(O_3)$, $L(NO_x)$, ϵ_N and R_N=[NO]/[NO_2] from the precursors [O_3], [NO_x], [CO], [HCHO], [H_2O] and [CH_4] at given temperature, pressure and photolysis rates j_{NO_2} and j_{O_3}. The scheme is derived from the reduced set of (equivalent)

1. $O_3 + NO \rightarrow O_2 + NO_2$
2. $O_3 + HO_2 \rightarrow 2O_2 + OH$
3. $NO + HO_2 \rightarrow NO_2 + OH$
4. $O_3 + OH \rightarrow O_2 + HO_2$
5. $CO + OH(+O_2) \rightarrow CO_2 + HO_2$
6. $CH_4 + OH \rightarrow\rightarrow HCHO + HO_2$
7. $HCHO + OH(+O_2) \rightarrow CO + HO_2 + H_2O$
8. $OH + HO_2 \rightarrow H_2O + O_2$
9. $HO_2 + HO_2(+M) \rightarrow H_2O_2 + O_2$
10. $HO_2 + NO_2(+M) \rightarrow HNO_4$
11. $OH + NO_2(+M) \rightarrow HNO_3$
12. $O_3 + h\nu + H_2O \rightarrow 2OH.$
13. $NO_2 + h\nu + O_2 \rightarrow NO + O_3$

Denoting the equivalent two-body reaction rates $k_1 - k_{13}$, the partitioning of NO_x can be approximated by the expression R_N=[NO]/[NO_2]=$j_{NO_2}/k_1[O_3]$. Similarly, partitioning

ACPD
4, 2533–2568, 2004

between OH and HO_2 is given by

$$R_H = \frac{[OH]}{[HO_2]} = \frac{k_2[O_3] + k_3 \frac{R_N}{1+R_N}[NO_x]}{k_4[O_3] + k_5[CO] + k_6[CH_4] + k_7[HCHO]}.$$

Due to the uncertainty and infrequency of SONEX formaldehyde measurements, we assumed a constant [HCHO]=29 pptv (Jaegle et al., 2000) for these calculations, as well as a constant $[CH_4]$=1.7 ppmv. Photochemical steady state treatment of the HO_x budget reveals

$$[HO_2] = \left(R_1^2[NO_x]^2 + \frac{P(HO_x)}{2(R_H k_8 + k_9)} \right)^{\frac{1}{2}} - R_1[NO_x],$$

where $R_1=(k_{11}R_H+k_{10})/[4(1+R_N)(k_8R_H+k_9)]$ and $P(HO_x)=P(OH)+P(HO_2)$ is the production rate of HO_x. $P(HO_2)$ represents production from hydrocarbons such as formaldehyde and acetone and is set to a constant 190 pptv day^{-1}, and $P(OH)=2k_{12}[O_3][H_2O]$. In order to estimate ϵ_N we then approximate $P(O_3)$ and $L(NO_x)$ by

$$P(O_3) \equiv k_3[HO_2]\,[NO] \quad \text{and} \quad L(NO_x) \equiv k_{11}[NO_2][OH].$$

Net ozone production occurs through reaction 3 when the surplus NO_2 molecule is photolysed in reaction 13. Finally, ozone loss is given by

$$L(O_3) \equiv (k_2[HO_2] + k_4[OH] + k_{12}[H_2O])\,[O_3].$$

5.2. Full scheme

The full scheme was introduced as due to the many neglected reactions the UTLS scheme gives poor correlations with TOMCAT in the lower troposphere and in the tropics. In addition to the radical species calculated by the UTLS scheme, the methyl-

peroxy radical concentration [CH_3O_2] is also calculated from the UTLS precursor concentrations, exploiting the extra reactions

6*b*. $CH_4 + OH(+O_2) \rightarrow CH_3O_2 + H_2O$
14. $CH_3O_2 + HO_2 \rightarrow O_2 + CH_3OOH$
15. $CH_3O_2 + NO(+O_2) \rightarrow\rightarrow NO_2 + HCHO + HO_2$.

The scheme is not extended to include a treatment of non-methane hydrocarbons, as we expect the sensitivity to mixing of these species and their oxidation products to be similar to that associated with methane. The accuracy of the PCSS expressions is extended, however, by taking $R_N = j_{NO_2}/(k_1[O_3]+k_2[HO_2]+k_{15}[CH_3O_2])$ and

$$R_H = \frac{\frac{P(OH)}{[HO_2]} + k_2[O_3] + \frac{R_N}{1+R_N} k_3[NO_x]}{k_4[O_3] + k_5[CO] + k_{6b}[CH_4] + k_7[HCHO]},$$

where P(OH) is as given for the UTLS scheme above, and

$$[HO_2] = \left(X^2 + \frac{P(HO_x)}{2(R_H k_8 + k_9)}\right)^{\frac{1}{2}} - X$$

with $X = R_1[NO_x] + R_2[CH_3O_2]$, R_1 as above and $R_2 = k_{14}/[4(R_H k_8 + k_9)]$. The methylperoxy radical concentration is then

$$[CH_3O_2] = \frac{k_{6b}[CH_4][OH]}{k_{15}[NO] + k_{14}[HO_2]}.$$

Ozone production $P(O_3)$ is $P(O_3) \equiv k_3[HO_2]\,[NO] + k_{15}[CH_3O_2][NO]$ (reaction 15 generates a surplus NO_2 molecule as with reaction 3). $L(NO_x)$ is as for the UTLS method above. An iterative method is used to evaluate the full scheme expressions consistently. As shown in Fig. 1 this extended scheme has the advantage of significantly improved correlations with the full TOMCAT chemistry throughout the troposphere.

Acknowledgements. J. G. Esler was supported by NERC Fellowship No. NER/I/S/1999/00137. Thanks to T. Kentarchos, K. Law, and R. Crowther for helpful comments on an earlier version.

References

Brunner, D., Staehelin J., and Jeker D.: Large-scale nitrogen oxide plumes in the tropopause region and implications for ozone, Science, 282, 1305–1309, 1998. 2550

Brunner, D., Staehelin J., Rogers H. L., et al.: An evaluation of the performance of chemistry transport models by comparison with research aircraft observations, Part 1: Concepts and overall model performance, Atmos. Chem. Phys. Disc., 3, 2499–2545, 2003. 2541, 2551

Chatfield, R. B. and Delaney A. C.: Convection links biomass burning to increased tropical ozone: However, Models will tend to overpredict O_3, J. Geophys. Res., 95, 18 473–18 488, 1990. 2535

Cobb, M.: Numerical modelling of oxidising processes in the troposphere, PhD thesis, University of Cambridge, 2002. 2549

Crowther, R. A., Law, K. S., Pyle, J. A., Bekki, S., and Smit, H.: Characterising the effect of large-scale model resolution on the calculated OH production using MOZAIC data, Geophys. Res. Lett., 29, doi:10.1029/2002GL014660, 2002. 2540, 2544, 2547

DeMore, W. B., Sander, S. B., Golden, D. M., et al.: Chemical kinetics and photochemical data for use in stratospheric Modeling, Jet Propul. Lab. Publ. 97–4, 1997. 2541

Esler, J. G., Tan, D. G. H., Haynes, P. H., Evans, M. J., Law, K. S., Plantevin, P.-H., and Pyle, J. A.: Stratosphere-troposphere exchange: Chemical sensitivity to mixing, J. Geophys. Res., 106, 4 717–4 731, 2001. 2535

Jacob, D. J., Logan, J. A., Yevich, R. M., et al.: Simulation of Summertime Ozone over North America, J. Geophys. Res., 98, 14 797–14 816, 1993. 2535, 2552

Jaegle, L., Jacob, D. J., Brune, W. H., et al.: Photochemistry of HOx in the upper troposphere at northern midlatitudes, J. Geophys. Res., 105, 3877–3892, 2000. 2554

Kentarchos, A. S., Roelofs G. J., and Lelieveld, J.: Simulation of extratropical synoptic-scale stratosphere-troposphere exchange using a coupled chemistry-GCM: Sensitivity to horizontal resolution, J. Atmos. Sci., 57, 2824–2838, 2000. 2537, 2542, 2546, 2550

Kraabøl, A. G., Flatøy, F., and Stordal., F.: Impact of NO_x emissions from subsonic aircraft: Inclusion of plume processes in a three-dimensional model covering Europe, North America and the North Atlantic, J. Geophys. Res., 105, 3573–3582, 2000. 2552

Lanzendorf, E. J., Hanisco, T. F., Wennberg, P. O., Cohen, R. C., Stimpfle, R. M., and Anderson, J. G.: Comparing atmospheric $[HO_2]/[OH]$ to modeled $[HO_2]/[OH]$: Identifying discrepancies with reaction rates, Geophys. Res. Lett., 28, 967–970, 2001.

Law, K. S., Plantevin, P.-H., Thouret, V., Marenco, A., Asman, W. A. H., Lawrence, M., Crutzen, P. J., Muller, J.-F., Hauglustaine, D. A., and Kanakidou, M.: Comparison between global chemistry transport model results and Measurement of Ozone by Airbus In-Service Aircraft (MOZAIC) data, J. Geophys. Res., 105, 1503–1525, 2000. 2552

Lelieveld, J. and Dentener, F.: What controls tropospheric ozone?, J. Geophys. Res., 105, 3531–3551, 2000. 2552

Lin, X., Trainer, M., and Liu, S. C.: On the nonlinearity of tropospheric ozone production, J. Geophys. Res., 93, 15 879–15 888, 1988. 2535

Liu, S. C., Trainer, M., Fehsenfeld, F. C., Parrish, D. D., Williams, E. J., Fahey, D. W., Hübler, G., and Murphy, P. C.: Ozone production in the rural troposphere and the implications for regional and global ozone distributions, J. Geophys. Res., 92, 4191–4207, 1987. 2535, 2536

O'Connor, F. M., Law, K. S., Pyle, J. A., Barjat, H., Brough, N., Dewey, K., Green, T., Kent, J., and Phillips, G.: Tropospheric ozone budget: regional and global calculations, Atmos. Chem. Phys. Discuss., 4, 991–1036, 2004. 2549

Plantevin, P.-H.: The oxidising capacity of the troposphere, PhD Thesis, University of Cambridge, 1999. 2543, 2548

Poppe, D., Zimmermann, J., and Dorn, H. P.: Field data and model calculations for the hydroxyl radical, J. Atmos. Sci., 52, 3402–3407, 1995. 2553

Poppe, D., Koppmann, R., and Rudolph, J.: Ozone formation in biomass burning plumes: Influence of atmospheric dilution, Geophys. Res. Lett. 25, 3823–3826, 1998. 2535

Prather, M. J.: Lifetimes and eigenstates in atmospheric chemistry, Geophys. Res. Lett., 21, 801–804, 1994. 2552

Pyle, J. A. and Zavody, A. M.: The modelling problems associated with spatial averaging, Q. J. R. Meteorol. Soc., 116, 753–766, 1990. 2535

Roeckner, E., Arpe, K., Bengtsson, L., et al.: The atmospheric general circulation model ECHAM4: Model description and simulation of present day climate, Rep. 218, Max-Planck Inst. for Meteorol., Hamburg, Germany, 1996. 2542

Roelofs, G. J. and Lelieveld, J.: Model study of the influence of cross-tropopause O_3 transports on tropospheric O_3 levels, Tellus, 49B, 38–55, 1997. 2543

Roelofs, G. J. and Lelieveld, J.: Tropospheric ozone simulation with a chemistry-general circulation model: Influence of higher hydrocarbon chemistry, J. Geophys. Res., 105, 22 697–22 712, 2000. 2542

Stockwell, D. Z. and Chipperfield, M. P.: A tropospheric chemical transport model: Development and validation of tmodel transport schemes, Q. J. R. Meteorol. Soc., 125, 1747–1783, 1999. 2542

Sillman, S., Logan, J. A., and Wolfsy, S. C.: A regional scale model for ozone in the United States with a subgrid representation of urban and power plant plumes, J. Geophys. Res., 95, 5731–5748, 1990. 2552

Thouret, V., Cho, J., Newell. R., Marenco, A., and Smit, H.: General characteristics of tropospheric trace constituent layers observed in the MOZAIC program, J. Geophys. Res., 105, 17 379–17 392, 2000. 2537

Tiedtke, M.: A comprehensive mass flux scheme for cumulus parameterisation in large-scale models, Mon. Weather Rev., 117, 1779–1800, 1989. 2537

Wild, O. and Prather, M. J.: Excitation of the Primary Tropospheric Chemical Mode in a Global Three-Dimensional Model, J. Geophys. Res., 105, 24 647–24 660, 2000. 2552

Wild, O., Prather, M. J., and Akimoto H.: Indirect long-term global cooling from NOx emissions, Geophys. Res. Lett., 28, 1719–1722, 2001. 2552

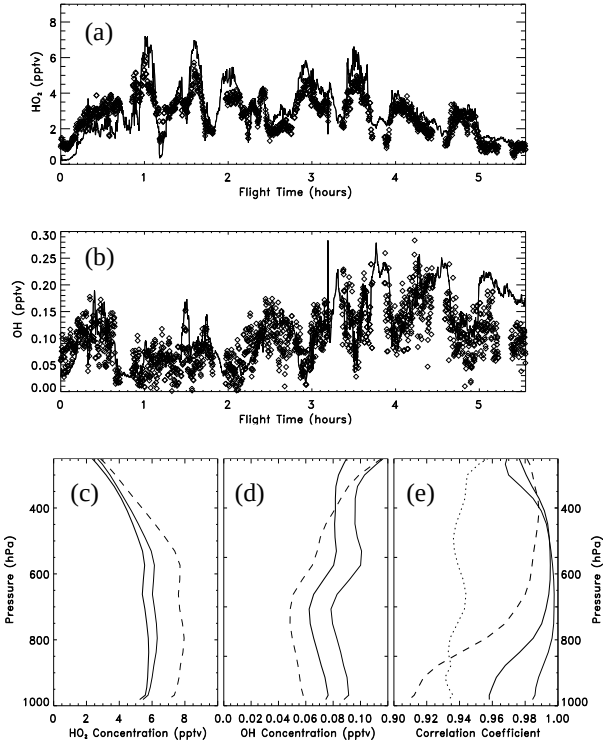

Fig. 1. **(a)** Measured [HO_2] (diamonds) and calculated [HO_2] from the UTLS scheme (curve) against flight time for SONEX flight 13. Measured O_3, NO, CO, H_2O, $j_{O(^1D)}$ and j_{NO_2} are used to make the calculations. **(b)** As (a) but for [OH]. **(c)** Global Mean TOMCAT [HO_2] against pressure from the low resolution experiment (thick solid line) compared with calculated [HO_2] from the UTLS scheme (dashed line) and the full scheme (thin solid line). Calculations are restricted to solar zenith angles <75°. **(d)** As (c) but for [OH]. **(e)** Correlations between TOMCAT [OH] and calculated [OH] for the full scheme (thin solid curve) and the UTLS scheme (dotted curve), and between TOMCAT [HO_2] and calculated [HO_2] for the full scheme (thick solid curve) and the UTLS scheme (dashed curve).

ACPD
4, 2533–2568, 2004

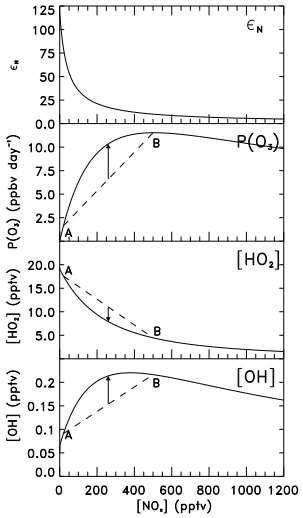

Fig. 2. Dependence of ϵ_N (ratio of O_3 molecules produced to NO_x molecules destroyed), $P(O_3)$, $[HO_2]$ and [OH] on $[NO_x]$ in the UTLS chemistry scheme described in the appendix. Reaction rates used are from TOMCAT at 250 K and 500 hPa, and photolysis rates are mean daytime (solar zenith angle <75°) values during SONEX ($j_{O(^1D)}=1.598\times10^{-5}\,s^{-1}$; $j_{NO_2}=8.824\times10^{-3}\,s^{-1}$). All calculations are for $[O_3]$=50 ppbv, [CO]=100 ppbv and $[H_2O]$=750 ppmv. A and B refer to two air parcels with $[NO_x]$=20 pptv and 500 pptv respectively. The dotted lines show the possible mean concentrations of [OH] and $[HO_2]$ between A and B assuming all possible ratios in size between the parcels. The arrows show the net change in mean concentrations of [OH] and $[HO_2]$, and rate of $P(O_3)$, in the two parcels due to complete mixing.

ACPD
4, 2533–2568, 2004

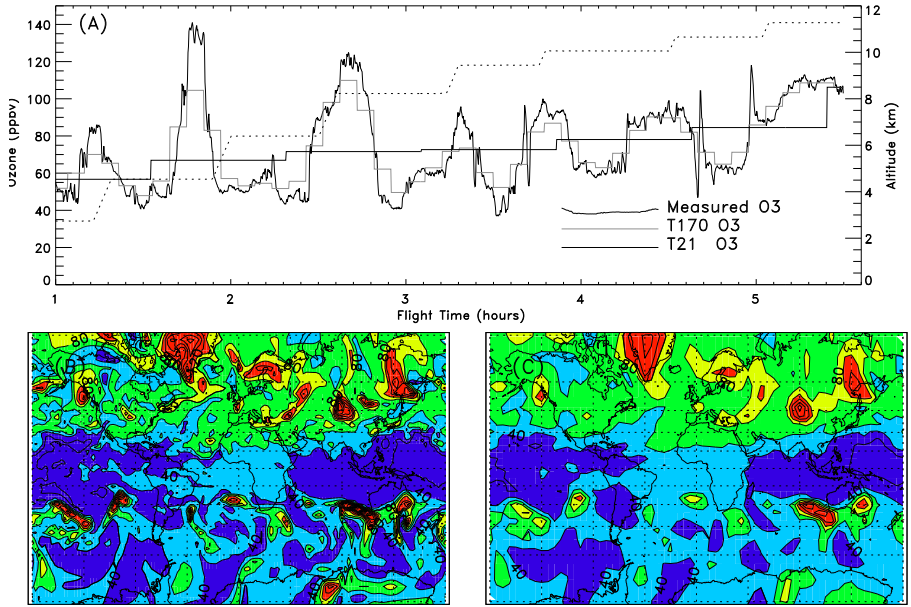

Fig. 3. (a) Ozone in ppbv measured along SONEX flight 13 (black curve) along with degraded ozone fields derived from these measurements (see text). The black line corresponds to an averaging scale consistent with a chemical transport model with grid-box resolution 2.75° (T42), and the grey line corresponds to 0.688° (T170). **(b)** TOMCAT O_3 at T42 on model level 22 (~700 hPa) on 29 July 1996 at 18:00 UT. **(c)** Degraded ozone (O_3:T42D) calculated from the T42 field in (b).

ACPD
4, 2533–2568, 2004

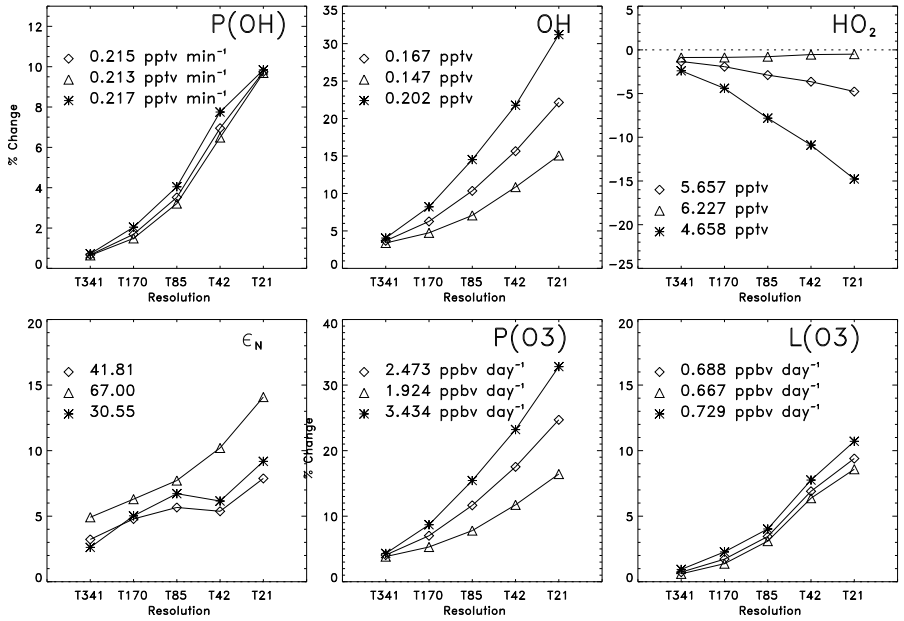

Fig. 4. Percentage change, relative to the values shown in each panel, of calculated radical concentrations and production/loss rates due to averaging the precursor fields O_3, NO_x, CO, H_2O over various scales (see text). Constant reaction rates (at 300 hPa, 240 K) and typical SONEX photolysis rates (see Fig. 1 caption) are used for the calculations. Diamonds correspond to all flights, triangles to flights mainly encountering marine air and stars to flights experiencing significant continental influence (see text).

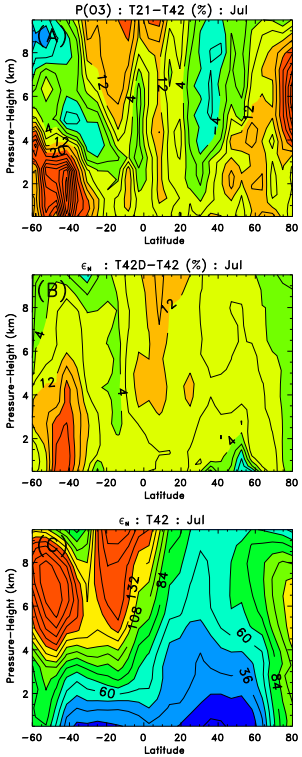

Fig. 5. (A) Difference in monthly mean $P(O_3)$ for July 1996 between the T21 and T42 TOMCAT simulations (contour interval ≡ c.i. 4%). **(B)** Percentage change in calculated ozone production efficiency ϵ_N when degraded (T42D) model fields are used in place of standard T42 model fields (c.i. 4%). **(C)** Monthly mean ϵ_N at T42 (c.i. 12).

ACPD
4, 2533–2568, 2004

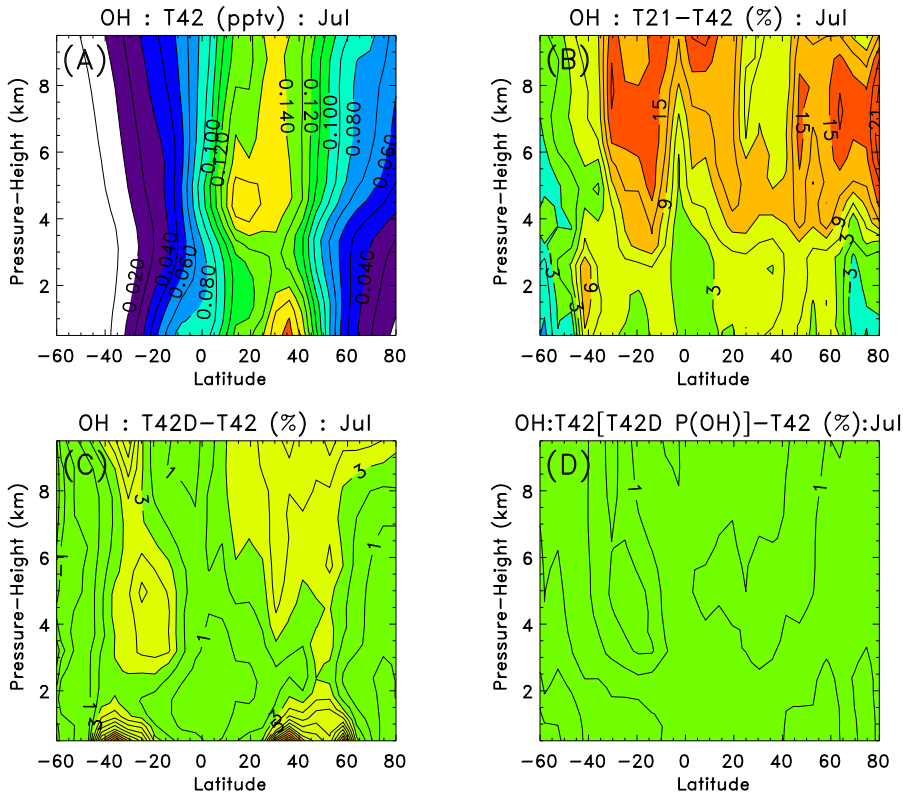

Fig. 6. (A) Monthly mean TOMCAT (T42) [OH] for July 1996 (c.i. 0.01 pptv). **(B)** Difference in [OH] between T21 and T42 simulations (c.i. 3%). **(C)** Percentage change in calculated [OH] when degraded (T42D) model fields are used in place of standard T42 model fields (c.i. 1%). **(D)** As (C), but with only *P*(OH) derived from degraded data (T42D) data. Colour levels are the same for panels (B)–(D).

ACPD
4, 2533–2568, 2004

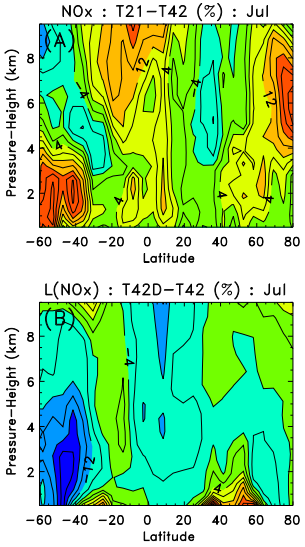

Fig. 7. (A) Differences in July 1996 monthly mean [NO_x] between the T21 and T42 TOMCAT simulations (c.i. 4%). **(B)** Percentage change in calculated L (NO_x) when degraded (T42D) fields are used in place of standard T42 fields (c.i. 4%).

ACPD
4, 2533–2568, 2004

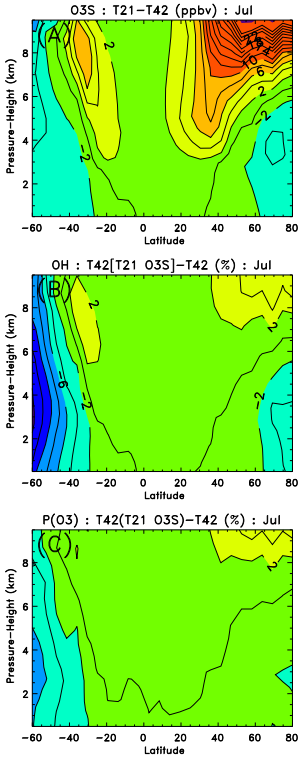

Fig. 8. (A) Differences in July 1996 monthly mean [O_3s] (stratospheric ozone tracer) between the T21 and T42 TOMCAT simulations (c.i. 2 ppbv). **(B)** Percentage change in calculated [OH] when T21 O_3s is used in place of T42 O_3s (c.i. 2%). **(C)** Percentage change in calculated $P(O_3)$ when T21 O_3s is used in place of T42 O_3s (c.i. 2%).

ACPD
4, 2533–2568, 2004

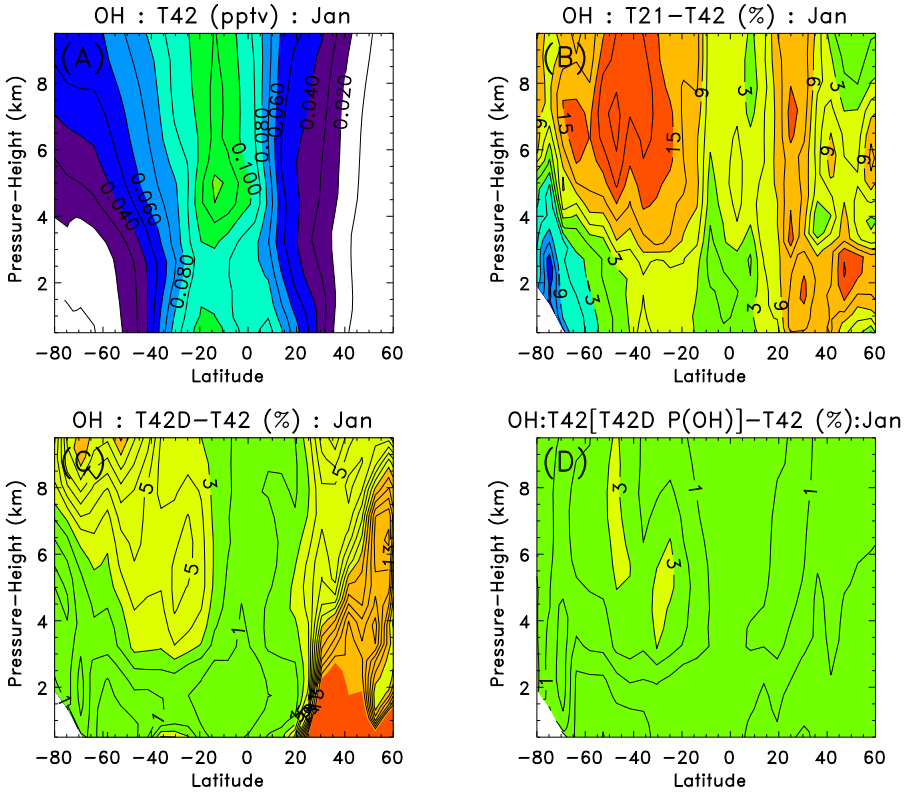

Fig. 9. As for Fig. 6 but for January 1996. **(A)** Monthly mean TOMCAT (T42) [OH] (c.i. 0.01 pptv). **(B)** Difference in [OH] between T21 and T42 simulations (c.i. 3%). **(C)** Percentage change in calculated [OH] when degraded (T42D) model fields are used in place of standard T42 model fields (c.i. 1%). **(D)** As (C), but with only *P*(OH) derived from degraded data (T42D) data.

ACPD
4, 2533–2568, 2004

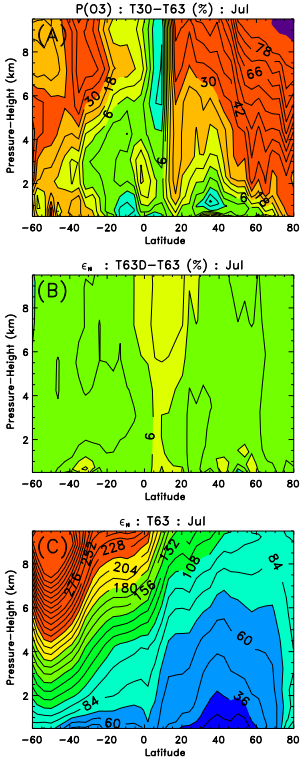

Fig. 10. As Fig. 5 but for T63 and T30 experiments in ECHAM4. **(A)** Difference in monthly mean $P(O_3)$ for July 1996 between the T30 and T63 ECHAM4 simulations (c.i. 4%). **(B)** Difference in calculated ϵ_N derived from the degraded (T63D) model fields and the calculated ϵ_N from the standard T63 model fields (c.i. 4%). **(C)** Monthly mean ϵ_N at T63 (c.i. 12).

ACPD
4, 2533–2568, 2004